Investigation on the Cutting Mechanism of Al/SiCp Composites in Ultrasonic Elliptical Vibration Machining

Wenxiang Chen
Shanghai University of Engineering Science
Xu Zhang (zxu1116@126.com)
Shanghai University of Engineering Science

Research Article

Keywords: Metal matrix composite, Ultrasonic elliptical vibration cutting, Cutting mechanism, Chip formation, Surface integrity, Finite element model machining

Posted Date: September 8th, 2021

DOI: https://doi.org/10.21203/rs.3.rs-868755/v1

Version of Record: A version of this preprint was published at The International Journal of Advanced Manufacturing Technology on March 19th, 2022. See the published version at https://doi.org/10.1007/s00170-022-08926-6.

Investigation on the cutting mechanism of Al/SiCp composites in ultrasonic elliptical vibration machining

Wenxiang Chen, Xu Zhang*

School of Mechanical and Automotive Engineering, Shanghai University of Engineering Science, Shanghai 201620, China.

Abstract: Aluminum (Al)-based silicon carbide (SiC) material composites are considered as difficult-to-machine materials because of the presence of hard reinforced SiC particles, which results in a greater cutting force and poor surface integrity during the machining process. This paper uses two finite element models to study the difference in the machining mechanism between ultrasonic elliptical vibration cutting (UEVC) and ordinary cutting (OC). Moreover, this paper mainly focuses on the influence of UEVC on cutting force, von Mises stress distribution, surface integrity, and chip formation. The models are validated by comparing chip shapes and machined surface features in OC machining Al/SiCp experience from the literature. Simulation results indicate that the cutting mechanism of Al/SiCp on UEVC is different from that of OC and has several good properties. At the same cutting parameters, high frequency vibration makes the cutting force of UEVC exhibit variable periodicity and reduces average cutting force. The instantaneous impact of tool and fast separation results in a more concentrated von Mises stress distribution, thereby resulting in the particles having a greater break degree than that obtained with OC. A comparison of the surface roughness values from the simulation result shows that UEVC obtains better surface integrity than OC does.

Keywords: Metal matrix composite, Ultrasonic elliptical vibration cutting, Cutting mechanism, Chip formation, Surface integrity, Finite element model machining

* Corresponding author.
Xu Zhang, School of Mechanical and Automotive Engineering, Shanghai University of Engineering Science, Shanghai 201620, China
E-mail address: zxu1116@126.com (Xu Zhang).

1. Introduction

Metal matrix composites consist of two or more kinds of different physical, chemical, and mechanical properties, and they may contain metal combined with another metal or other types of materials, such as ceramics or organic materials. Many kinds of metal matrix composites exist. Silicon carbide (SiC) particle-reinforced aluminum (Al) matrix composite is a metal matrix composite with reinforced particles and usually uses aluminum alloy or aluminum as the matrix and silicon carbide particles as the reinforced phase. In accordance with design requirements, a multiphase composite material is formed with an evident interface in a specific form, proportion, and distribution condition. The composite material has the excellent performances of two or more materials, such as high specific strength, stiffness, great wear resistance, and low coefficient of thermal expansion [1, 2]. Metal matrix composites are generally produced in a process close to the final shape, such as casting and forging. However, machining is a necessary stage to achieve high precision and complex structure. Silicon carbide particle is an ultra-hard material with a Mohs hardness of 9.5. With the high hardness and wear resistance of the reinforced particles distributed in the aluminum or aluminum alloy matrix, the tools exert a greater cutting reaction force during the machining process, thereby resulting in the Al/SiCp composite material having greater difference from conventional materials. Al/SiCp composite material possesses inhomogeneous and abrasion qualities. Tools undergo wear due to the material's ultra-hard and wear resistance and surface damage during the Al/SiCp reinforced particles' secondary machining. Such conditions are considered the main obstacles in the machining of Al/SiCp composite materials [3, 4].

Using the finite element simulation is a very effective method to study the cutting of materials. Compared with conventional experiment , the simulate method can be adjusted cutting

parameters conveniently, and the process can be simulated and verified repeatedly by modifying parameters. There are mainly two methods to simulate the cutting of Al/SiCp: (a) establishing homogeneous material model from a macro perspective, which without considering the micro structure of composite material and homogenizes the material properties. (b) establishing multiphase model from micro perspective, considering matrix and reinforced phase properties, shape of reinforced particles respectively. The homogeneous model has high efficiency and is suitable for simulating cutting force and temperature totally. The multiphase model has low efficiency but but it can observe the behavior of particles and obtain more accurate results. Y. Zhu et al. [5] established a plane-strain thermo-elasto-plastic finite element model with considering the interface failure mode between the aluminium matrix and alumina particles. He believed that details afforded by this finite element analysis will be of great importance for better understanding of the particle's behavior during machining of MMC and can help in optimizing the process parameters. Chunzheng Duan et al. [6] developed a three-phase friction model that considered the influence of matrix adhesion, two-body abrasion, three-body rolling and randomly distributed round particles.

Complex and severe distortion behavior during the machining of Al/SiCp composite material can be attributed to the elastoplastic deformation and ductile failure of the metal matrix, the elastic deformation and brittle crack of ceramic particles, and the debonding of particles from the matrix. A smooth surface can be obtained by completely removing the SiC particles from the aluminum matrix. When the fractured SiC particles remain in the aluminum matrix, the surface quality will improve. When the SiC particles fall off from the aluminum matrix, the surface quality will seriously deteriorate due to the formation of holes and cavity [7]. Wu et al. [8] studied the

influence of the shape and volume fraction of SiC particles on machining material condition and surface stress. They found that the existence of SiC reinforced particles is one of the critical factors that affect the surface processing quality and that dimension, shape, and volume fraction have an obvious influence on the machinability of Al/SiCp composite material. Wang et al. [9] established both a randomly distributed circular SiC particles model and a polygon SiC particles model were built respectively with high volume fraction. Studying the surface defect forming mechanism of machining Al/SiCp composite material and found that surface defects are generally attributed to the rotation, pulling-out, microfracture, and cutting-through of debonding SiC particles, which leave cavities and holes and scratches. Wang [10] investigated the underlying cutting mechanismof Al/SiCp. Using finite element simulations studied the effect of three types of fracture and the particle size.on machined surface properties.

Ultrasonic vibration cutting involves adding micronmeters-scale ultrasonic-frequency vibration to cutting tools, controlling the vibration frequency and vibration amplitude to make cutting tools vibrate in axial, radial, and tangential directions [11]. Doing so allows the tools to continuously change cutting speed direction and movement direction. As a result, the tools and workpiece separate periodically and achieve the effect of intermittent cutting. Unlike traditional cutting, ultrasonic vibration cutting has the characteristics of energy concentration and instantaneous cutting. A transient thermal mechanical coupling finite element model of traditional and ultrasonic cutting of elastic–plastic materials has been established to study the effect of ultrasonic vibration orthogonal turning on difficult-to-machine materials like Ti6Al4V [12, 13], stainless steel [14] and NiCr alloy [15]. Findings show that the average cutting force and cutting temperature values of ultrasonic vibration cutting were generally reduced, and different chip

formation mechanism was analyzed. The reduced cutting force restrained burrs and local microcracks, thus helping improve the machining quality of microfeatures. Wei Bai et al. [16] studied the ultrasonically assisted cutting (UAC) on machined surface and chip of Ti6Al4V alloy. The result demonstrated a lower level of surface damage in UAC compared with OC. Zheng W [17] also founded the scratched surface of Al/SiCp in traditional scratch (TS) process was damaged to a greater degree than that subjected to ultrasonic vibration assisted scratch (US) test process. With the assistance of ultrasonic vibration, scratch force and friction coefficient in US process were smaller than those in TS process, and the reduction of them was modeled and analyzed.

As a special ultrasonic vibration machining method, UEVC has the function of ironing and finishing the workpiece by using a chip separated from the tool and high-frequency intermittent cutting. The overlapping effect of two adjacent elliptical tracks in the feed direction reduces the height difference of the surface and improves the surface quality. Under the same cutting parameters, the appropriate ultrasonic amplitude has a positive effect on the surface micromorphology [18]. Tan R [19] used UEVC to process Ti-6Al-4V alloy microgrooves. The results showed that UEVC significantly reduced the expansion and springback of the material, and improved the surface integrity of the material. In addition, when the TSR (ratio of nominal cutting speed to peak horizontal vibration speed) was properly selected, the accuracy of microgrooves reached 98% and the roughness value was about 0.1 μm. In this process, the chip is subjected to upward friction on a part of the tool ellipse path, which can significantly reduce the cutting resistance. The chip shape is different from the traditional flat chip because of the small average cutting force. Unlike the Al/SiCp model of the plastic matrix studied in this paper, SiC-S is a

high-strength, high-hardness matrix with plastic reinforcement. Studies show that a larger amplitude in the cutting direction or a smaller amplitude in the depth of the cutting direction and a higher frequency were beneficial to improve the ductile machinability of Rb-SiC in UEVC [20]. Daxi Geng [21] found that less delamination damage and higher processing efficiency can be achieved in rotary ultrasonic elliptical machining compared with core drilling.

Although ultrasonic vibration has been proven to be able to improve the machinability of a variety of difficult-to-machine materials, little research has been conducted on the combination of UEVC of Al/SiC, which has a plastic matrix and brittle reinforcement. So, this study established a multiphase workpiece model of SiC particle reinforced aluminum matrix composites, the model combines the aluminum matrix model with Johnson Cook constitutive model, SiC particle model that considered brittle crack, and the cohesive element model simulating the traction between particles and matrix, therefor, the model can simulate the damage of Al/SiCp and the connection of particles and matrix. the removal mechanisms of OC and UEVC machining Al/SiCp were compared, and the effect of UEVC on tool–particle interaction was studied, which involved the variation of cutting force, chip formation, distribution of von Mises stress, and profile of the machined surface.

2. Methodology

2.1. Trajectory of ultrasonic elliptical vibration cutting

The track of UEVC usually consists of two parts.

$$\begin{cases} X(t) = A\cos(2\pi ft) \\ Y(t) = B\cos(2\pi ft + \phi) \end{cases} \tag{1}$$

where X (t) and Y (t) are the coordinate of the point on the tool tip moving along the cutting direction and the cutting depth direction on the elliptical trajectory, respectively; A and B are the corresponding vibration amplitude in the two directions; and F , t , ϕ are the amplitude, time, and phase shift, respectively. The parameter ϕ affects the shape of the ellipse, as shown in Fig. 1. Gi Dae Kim [22] defined an index termed non-contact index (NCI) involving the vibration amplitude of the elliptical locus to determine the existence of cyclic breaking of the contact under a given UEVC condition. In this paper, the vibration phase difference between the cutting direction and the cutting depth direction is 90°, and the trajectory is a standard ellipse with A and B axes.

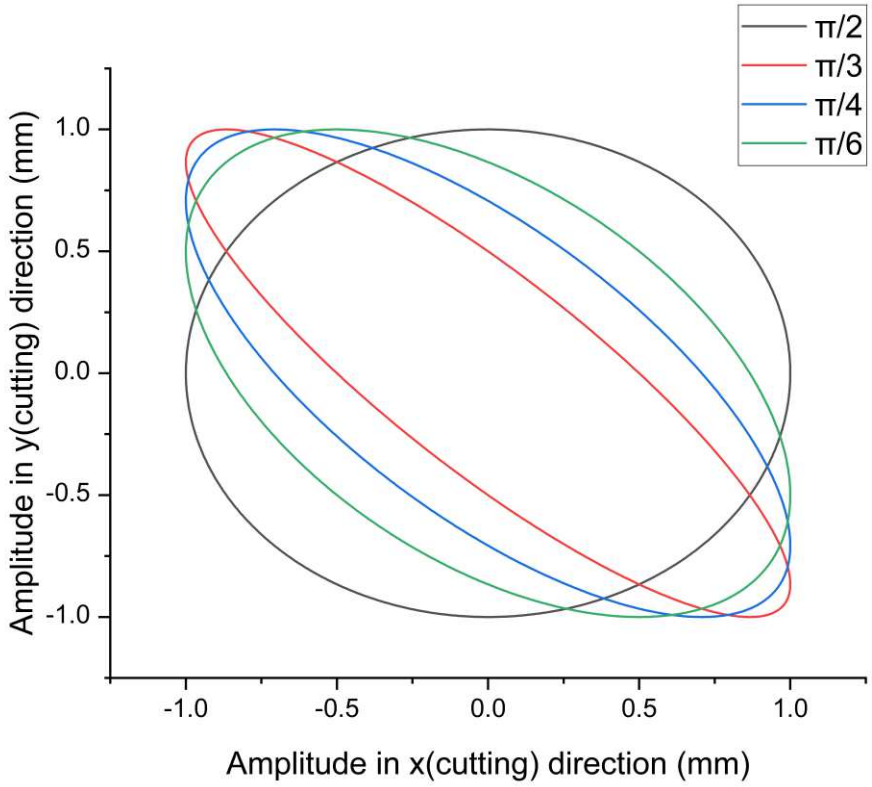

Fig. 1 Effect of different ϕ on the elliptical locus.

The trajectory of the tool relative to the workpiece is shown in Fig. 2, and the equation is as follows:

$$\begin{cases} X(t) = A\cos(2\pi ft) + \mathrm{vt} \\ Y(t) = -B\sin(2\pi ft) \end{cases} \tag{2}$$

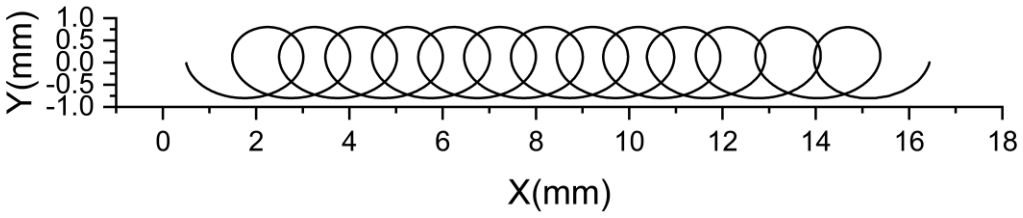

Fig. 2 Simulated trajectory of the tool in the UEVC process.

Figure 3 shows a schematic of the typical UEVC process, in which the tool feeds at a normal cutting speed and moves along the elliptical path under the action of vibration. The process can be divided into three parts: (a) In the a–b stage, the tool approaches the workpiece; (b) In the b–c stage, the tool penetrates the workpiece; (c) In the c–a stage, the tool returns to the initial position. The vibration speed of the tool should be greater than the feed speed of the workpiece to achieve intermittent cutting. When the maximum tool elliptical vibration speed in the cutting direction is greater than the cutting speed, then the process is considered intermittent cutting. When the maximum tool elliptical vibration speed in the cutting direction is smaller than the cutting speed, then the process is considered continuous cutting.

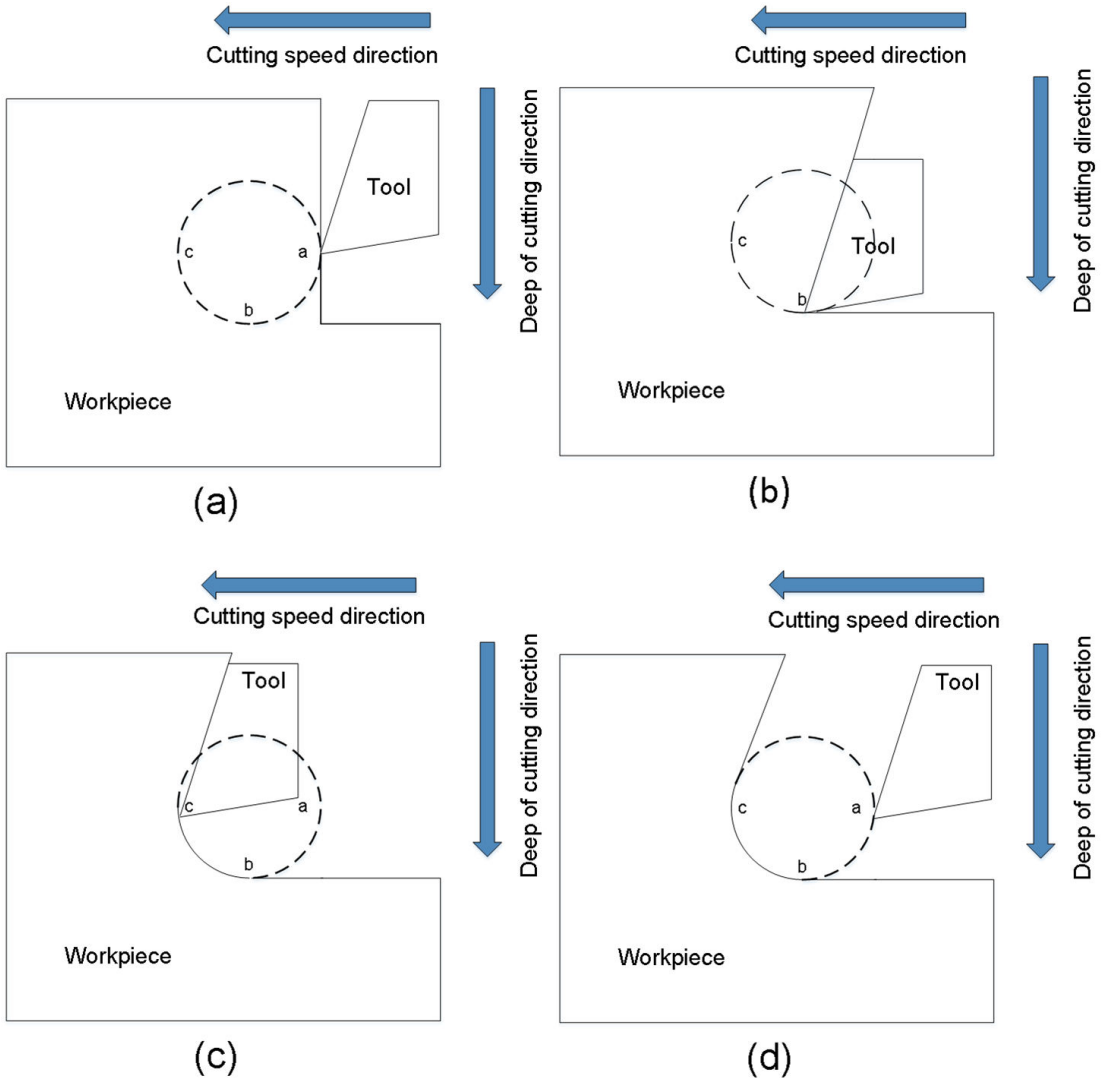

Fig. 3 Schematic of elliptical vibration cutting.

2.2. Simulation of ultrasonic elliptical vibration cutting machining Al/SICp

Figure 4 shows the finite element model of conventional machining and UEVC machining of Al/SiCp. The workpiece length and height are 0.14 and 0.056 mm, respectively. The aluminum matrix and reinforced SiC particles are modeled separately and then combined in assembly module. The model is established refer to the references [23], so the SiC particles is simplified as circle with a 0.01 mm diameter and a volume fraction of 10% rather than random polygons. The reinforced SiC particles are distributed evenly in the cutting path of the model, thus ensuring that three kinds of connect situation are fully considered. The rake and flank angle of the tool are 10°

and 6°, respectively; the radius of the tool tip is 0.001 mm; and the tool is set as an analytical rigid body, which is consistent with the reference

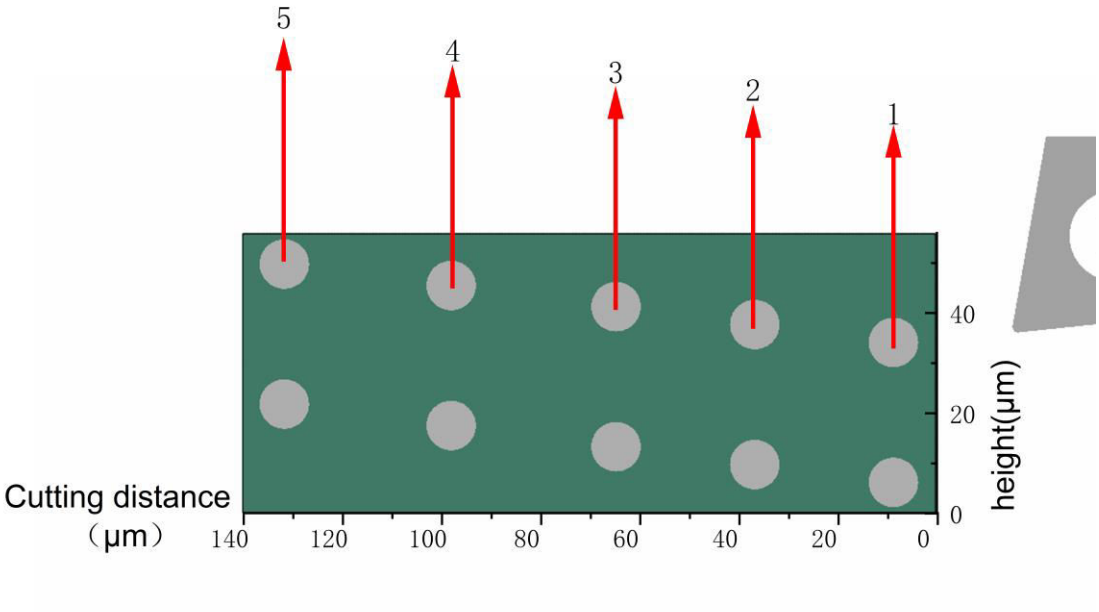

Fig. 4 FE geometry model for cutting of Al/SiCp composites with 10% particle volume fraction and a particle diameter of 10 μm.

2.3. Material property

During the machining process, the elastic–plastic deformation of the workpiece occurs under high temperature and large strain. Thus, the Johnson-Cook (J-C) constitutive equation is selected, which can reflect the effect of strain and strain rate on material flow stress.

$$\overline{\sigma} = \left[A + B\left(\overline{\varepsilon}^{pl}\right)^{n} \right] \left[1 + C \ln \left(\frac{\dot{\overline{\varepsilon}}^{pl}}{\dot{\varepsilon}_0} \right) \right] \left[1 - \left(\frac{T - T_{room}}{T_{melt} - T_{room}} \right)^{m} \right] \tag{3}$$

where $\overline{\sigma}$ denotes the flow stress, $\overline{\varepsilon}^{pl}$ refers the plastic strain, $\dot{\overline{\varepsilon}}^{pl}$ is the plastic strain rate, $\dot{\varepsilon}_0$ indicates the reference strain rate set as 1e-6 s^{-1} in the millimeter unit system, T is the temperature of the workpiece , T_{melt} indicates material melting, and T_{room} indicates ambient temperatures. Coefficient A is the yield strength, B denotes the hardening modulus, C represents the strain rate sensitivity coefficient, n indicates the hardening coefficient, and m is the thermal softening coefficient. In general, the material constant is achieved from static tensile tests, torsion tests, and dynamic Hopkinson bar tensile tests. Table 1 lists the material properties and J-C constitutive equation model parameters of the aluminum matrix used in this work.

The aluminum matrix is set as a variable elastic–plastic material with fracture failure criterion. The J-C fracture failure formula is used to define the chip separate criterion during the simulation of the machining process, and equivalent plastic strain $\overline{\varepsilon}_f^{pl}$ is used to judge whether fracture occurs or not. When parameter D is equal to unity, failure occurs and the corresponding element is deleted. The failure parameter D can be defined as follows:

$$D = \sum \frac{\Delta \overline{\varepsilon}^{pl}}{\overline{\varepsilon}_f^{pl}} \tag{4}$$

where $\Delta \overline{\varepsilon}^{pl}$ is the equivalent plastic strain increment of each iteration, and $\overline{\varepsilon}_f^{pl}$ is the equivalent strain when material fracture.

The equivalent strain of material failure is calculated by the following formula:

$$\overline{\varepsilon}_f^{pl} = \left[d_1 + d_2 \exp d_3 (\frac{P}{\sigma}) \right] \left[1 + d4 \ln \left(\frac{\dot{\overline{\varepsilon}}^{pl}}{\dot{\varepsilon}_0} \right) \right] \left[1 + d5 \left(\frac{T - T_{room}}{T_{melt} - T_{room}} \right) \right] \tag{5}$$

where $\dot{\varepsilon}_0$ indicates the reference strain rate, $\frac{P}{\sigma}$ is the stress triaxiality , $\dot{\bar{\varepsilon}}^{pl}$ indicates the plastic strain rate, and $d_1 - d_5$ are the fracture parameters acquired from tensile and torsional tests in an environment lower than the convert temperature.

Brittle fracture damage model is used to simulated reinforced SiC particle brittle fracture in Abaqus, and maximum normal stress is used to judge whether cracks appeared or not. The criteria is defined as follows:

$$\max(\sigma_1, \sigma_2, \sigma_3) = \sigma_0 \tag{6}$$

Subscripts 1,2,3 are the principal stress components, and subscript 0 is the tensile strength of materials.

After brittle crack, the post failure behavior of SIC particle is defined by a stress–strain relationship. Mode I indicates tensile fracture behavior, and mode II indicates shear fracture behavior. Crack production is based on mode I, but the post-crack behavior includes mode I and II, and the shear modulus G of material decreases with the crack opening. The shear modulus G_c after crack opening is defined as a linear function of crack opening strain e_{nn}^{ck} by using the shear force retention model

$$Gc = \left(1 - \frac{e_{nn}^{ck}}{e_{\max}^{ck}}\right)^P G \tag{7}$$

The crack opening strain is defined as the strain when the material fails, and the maximum crack cracking strain is 10 times the crack cracking strain. Other relevant parameters are shown in Table 2.

2.4 Cohesive zone model

A comparison of homogeneous materials and multiphase materials shows that the connection between particles and matrix is need to be considered, correct simulation of the transmission of force and traction between particles and matrix plays an important role in the evolution of particles reinforced mateirals during machining. A cohesive zone model is mainly used to simulate the bond interface. The failure zone is assumed to have zero thickness at the initial state. This zone consists of two same surface. Then, under the predetermined load, the separation is determined by the traction separation law. A cohesive element is usually used to describe the ideal traction shift behavior to simulate interfacial debonding, transgranular failure, and intergranular fracture [24]. Research used four different finite element models with or without separation line and with or without a cohesive element to study the orthogonal cutting process of Al/SICp, and variables such as cutting force, temperature, stress distribution, and shape of the chip were predicted successfully. The cohesive element model can well simulate the debonding behavior of reinforced particles [25]. Therefore, a cohesive element is inserted between the aluminum matrix and the reinforced SiC particles to simulate the bond function

between the matrix and the reinforced particles in metal matrix composites in this paper.

The failure of the cohesive element has several criteria. The maximum principal stress failure criterion is used in this paper, which assumes that failure begins when the maximum nominal stress reaches a predetermined value. When fracture energy or displacement reaches the predetermined value, the cohesive element is deleted. After the workpiece is in contact with the tool, whether the particles leave with the chips of the aluminum matrix or stay in the matrix due to the interface bonding force depends on whether the cohesive elements are damaged. Currently, the cohesive element cannot simulate the variation of temperature. Therefore,selecting the cohesive separation parameters-the traction of modes I and II at cutting temperature as the maximum stress corresponding to the traction separation behavior of the bonded structure. The relative parameters are shown in Table 3.

Table 1. Material properties for Al [23].

Parameters	Values
Density (ton/mm3)	2820×10^{-12}
Young's modulus (MPa)	70,600
Poisson's ratio	0.35
T_{melt} (K)	900
$T_{transition}$ (K)	290
A	224
B	426
n	0.2

m	0.859
C	0.003
d1	0.13
d2	0.13
d3	-1.5
d4	0.011
d5	0

Table 2. Material properties for SiC particles [23].

Parameters	Values
Density (ton/mm3)	3200×10^{-12}
Young's modulus (MPa)	408000
Poisson's ratio	0.35
Tensile stress (MPa)	3900

Table 3. Cohesive zone model properties [25]

Maximum model Ⅰ traction (GPa)	Maximum model Ⅱ traction (GPa)
2.42	1.76

2.5. Friction model

In this paper, the Coulomb friction model is used to simulate the connection relationship among the cutting tool, aluminum matrix, and SiC particles. The friction model is defined as follows:

$$\tau_f = \begin{cases} \mu\sigma_n & when\ \mu\sigma_n < \tau_{\max} \\ \tau_{\max} & when\ \mu\sigma_n > \tau_{\max} \end{cases} \tag{8}$$

This model has been used in many cutting simulations, where σ_n is the model normal stress of tool–chip contact, μ is the friction coefficient, τ_f is the shear stress, and $\tau_{\max}$ is the maximum value of shear stress. According to the reference [23], the friction coefficient of whole workpiece is 0.5 in this paper, and the maximum value of shear stress is 224 MPa, which is yield stress of the material, Once the τ_f at the interface reaches $\tau_{\max}$, the friction state between the tool and the workpiece changes from bonding friction to sliding friction

2.6. Simulation setting

The finite element model is established by the general finite element software Abaqus. The model uses an explicit dynamic analysis program, and the three-dimensional simplified integral unit (C3D8R) is gridded to the particles and the substrate. The number of units is approximately 28,000, and the cohesive zone model uses zero-thickness cohesive elements.

In the common cutting model, the tool is fixed and the workpiece moves uniformly at a predetermined speed. In the UEVC model, the tool elliptical trajectory is realized by applying a different displacement in the cutting direction (X direction) and the depth of cut (DOC) direction (Y direction), where the X direction is 10 μm, and the Y direction is 8 μm. The positive and negative values of the displacement represent the movement in the positive and negative directions of the coordinate axis, respectively, and the workpiece moves at a constant speed of 200 mm/s. Ultrasonic elliptical vibration machining is simulated in some literature by fixing the workpiece and applying cyclic variable speed on the nominal cutting direction and the nominal DOC direction of the tool, respectively, to realize the elliptical vibration of the tool. The elliptical vibration path is realized by applying the cutting speed to the left side and the lower side of the

workpiece in the positive X direction and by applying periodic displacement to the tool in the X and Y directions, which can better simulate the real machining environment.

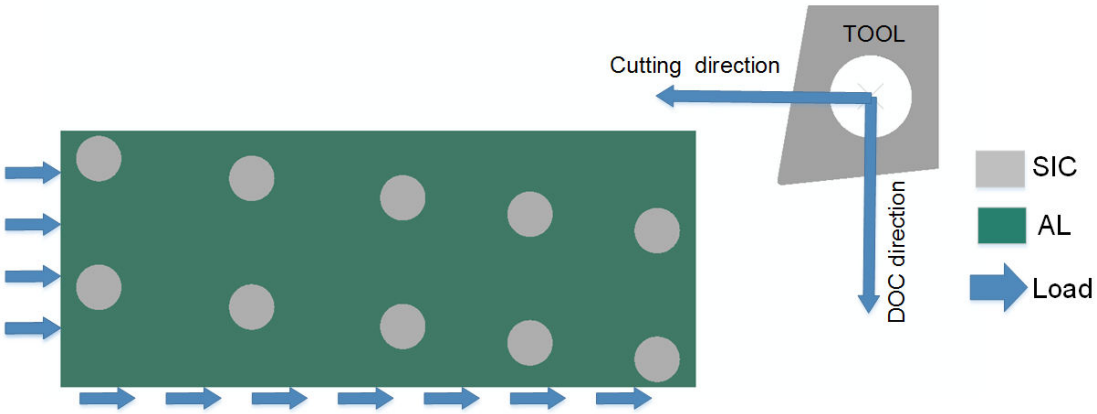

Fig. 5 Simulated load in the UEVC FE model.

3. Validation of the model

Xiangyu Teng et al. [23] simulated process of milling Al/SiCp and conducted milling experiment. Through comparing the machined surface teatures and chip shapes to verify. The result showed good consistency.

In this paper, in order to verify the accuracy of simulation, the OC and UEVC simulation models was established according to Xiangyu Teng's experimental condition by simulation software, and all cutting parameters were consistent with the experiment above-mentioned. Validating the accuracy of models through comparing the cutting force, chip shapes and machined surface features. Figure 6 shows the cutting force compared result of simulation and experiment. There are not much difference between them, and the maximum error was 12%, which can attributed to the difference of workpiece models and the distribution of SiC particles. Figure 7 shows the chip shapes and the machined surface compared result of simulation and experiment.

Through comparison, the saw-tooth discontinued chips shape of the simulation result was close to that in the actual cutting, the machined surface feature, like cavity and fragment SiC particle. Through setting and adjusting the simulation parameters reasonably, the simulated cutting condition can close to the experiment, the simulated result also can close to the experimental result. Although the data are not completely consistent, but error was within reasonably range.

Finally, changing the tool loads to simulate the UEVC machining process. Therefore, it can be considered that the established UEVC model can correctly simulate the actual machining.

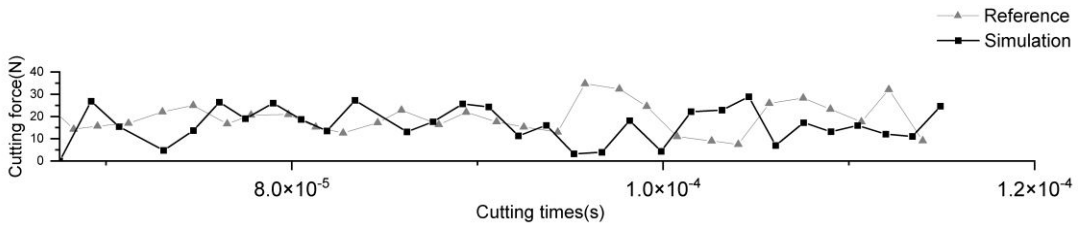

Fig. 6 Cutting force of simulation and reference [23] during OC machining Al/SiCp.

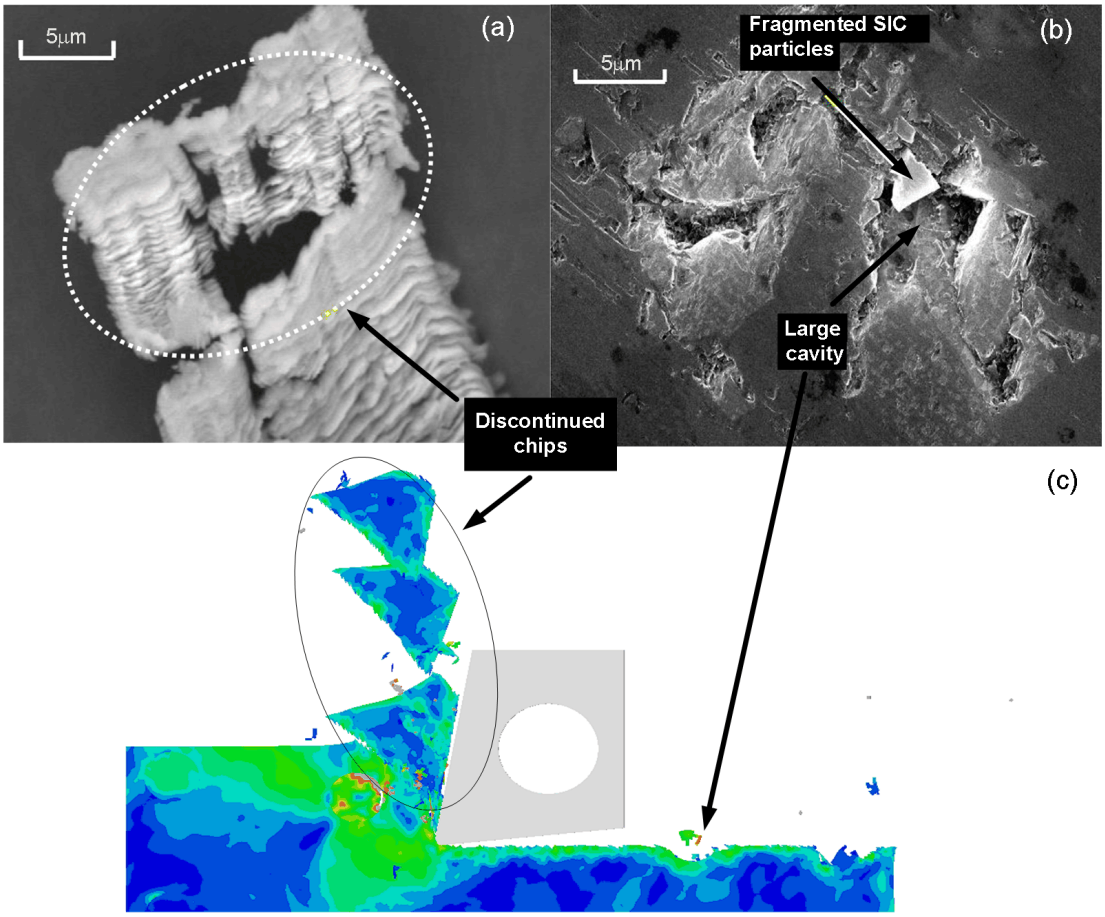

Fig. 7 SEM micrographs of (a) machined surface and (b) chips obtained from experimental works of 20 μm 10% volume fraction Al/SiCp [23], (c)OC simulation result.

4. Results and discussion

First, the Al/SiCp simulation of traditional turning and ultrasonic elliptical vibration turning is performed, and the cutting mechanism is explained. The vibration frequency is 20 kHz, the amplitude of the cutting direction is Ac = 10 μm, and the cutting depth is Ad = 8 μm. Figures 8a and 8b show the cutting path of the tool in the two machining models, respectively. Fig. 8 shows that the position relationship between the tool tip and each SiC particle is different. The process can be described as follows: 1) The tool tip's path passes through the top of the particle; 2) The tool tip's path passes through the center of the particle; 3) The tool tip's path

passes through the bottom of the particle; 4) The tool tip's path has no contact with the particle, but the rake face has contact with the particle; 5) The blade path has no contact with the particle.

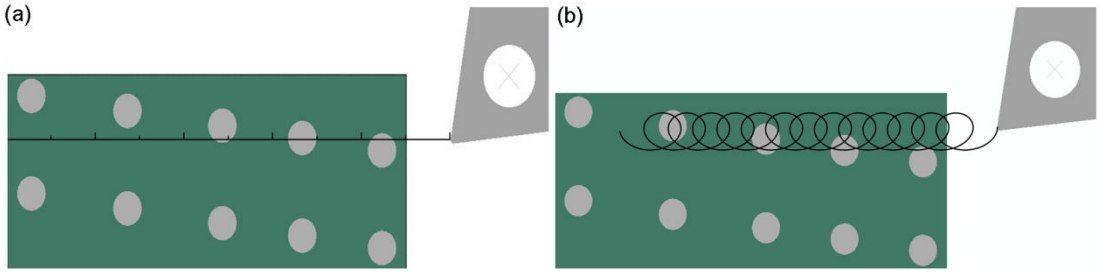

Fig. 8 Simulated cutting track in (a) OC; (b) UEVC FE mode

4.1. Comparison of the cutting forces of Al/SICp

Figures 9a and 9b show the change in the cutting force during the machining process under the two machining methods. The cutting force of the contact part between the SiC particles and the tool is shown as a dotted line.

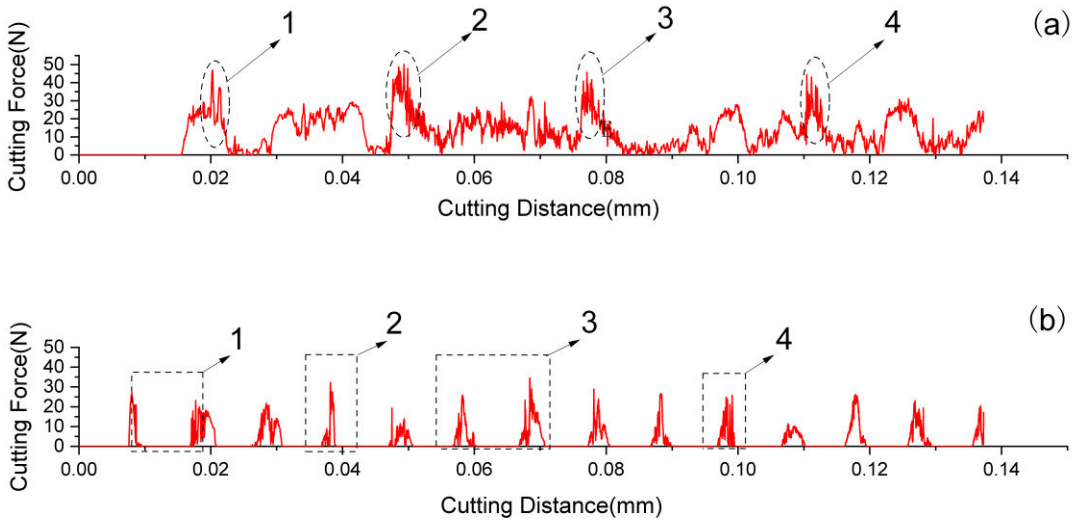

Fig. 9 Variation in simulated cutting force of Al/SiCp with cutting length in (a) OC; (b) UEVC.

In the two machining environments, the amplitude of the cutting force between the tool and the matrix is about 0.005 N. When the cutting edge is close to the SiC particles, the cutting force

increases rapidly and reaches the maximum value when cutting SiC particles. The maximum cutting force of OC is about 0.0125 N and that of UEVC is about 0.017 N, because the fracture toughness and Mohs hardness of SiC are higher than those of the aluminum matrix. Therefore, the cutting force is increased immediately when the cutting edge first cuts the SiC particle. After the brittle fracture of SiC particles, a transient non-contact state exists between the tool and the workpiece. Thus, the cutting force decreases sharply when the cutting edge passes through the SiC particle. The sharp fluctuation of the cutting force during Al/SiCp machining can be considered the result of the interaction between the cutting edge and the particles, such as the particle fracture, the matrix fracture, and the debonding of particles from the matrix.

In OC process, the average cutting force is about 0.0035 N. The cutting force curve increases after the cutting edge contacts with the particle. In accordance with the different positions of the cutter and the particle, the following different changes occur: As the tool cuts particle 1, the cutting force curve rises for a short time and has a large amplitude, while the cutting force curve trends of particles 2, 3, and 4 are similar, rising and staying for a longer time than particle 1 does and then declining slowly. On the one hand, the cutting force amplitude drops along with the debonding range drops of the particle from the matrix. On the other hand, during the cutting process, the cutting force consists of the resistance of the matrix and the particles, and the traction of the particle–matrix. When the fracture toughness of SiC particle is not satisfied, but cohesive element meets the failure criteria, the particle will debond from the matrix and move with the chip of the matrix. Afterward, the process is equivalent to continuous cutting, thereby forming a wider peak value curve.

In the UEVC process, the average cutting force is about 0.00068 N, which is a quarter of OC. First, the overall cutting force changes periodically, and the characteristics of UEVC make the average cutting force lower. Whether the aluminum matrix or the SiC reinforced particles are being cut, the cutting force amplitude is relatively close; the cutting force increases from contact to the peak value and decreases to zero as the tool exits the workpiece. Further research found that if the lowest point in the trajectory of the tool is considered the starting point of the tool path in the DOC direction, the cutting speed of the tool at the initial stage is smaller than the chip flow speed, and the direction is opposite the chip flow direction, thereby blocking chip flow. Then, the cutting speed of the tool in the DOC direction gradually increases. When the cutting speed exceeds the chip flow speed, the friction between chip and tool rake face is reversed. This feature is different from both of ordinary cutting andordinary vibration cutting. The friction direction is the same as the chip flow-out direction, thereby promoting the removal of the chip, resulting in the negative value of thrust force in a cutting cycle, thereby main cutting force also decrease, shown in fig 10.

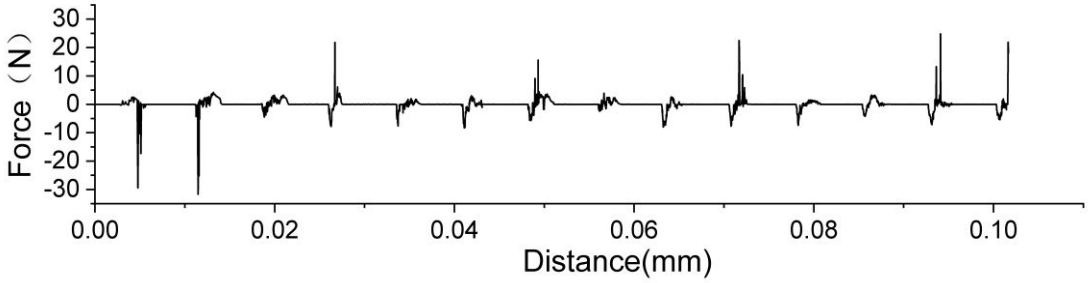

Fig. 10 Variation in simulated thrust cutting force of Al/SiCp with cutting length in UEVC.

4.2 Chip formation evolution

The distribution of stress during chip formation needs to be studied to analyze the effect of the two processing methods on chip formation. The cutting force curve of OC and previous studies showed that the relative position of the cutting edge and SiC particle has an important impact on

the variation of cutting force. Figure 12a shows that the contact part of the cutting edge and particle is at the upper part, which needs less fracture toughness. Thus, particle 1 experienced obvious brittle fracture, and crack formation and propagation occurred inside the particle with the rapid wave of cutting force. During the process, the particle cracks along the direction of stress concentration and extends to the other side. The cutting force curve reaches the local maximum value before crack formation then immediately drops to zero. As a result of the restrictive behavior of particle traction on the matrix, the shear plane appears in the matrix, and then a crack along with the shear plane extends to the top surface of the workpiece to form a chip. Figures 12b and 12c show that as the tool advances, the aluminum matrix around particles 2, 3, and 4 tears, leading to the debonding of the matrix particle interface. For particle 2, the contact part is at the middle, which needs maximum fracture toughness. Thus, the peak value of the cutting force curve appears here and lasts for a long time, but it does not reach the fracture toughness. Therefore, particle 2 is completely extracted from the matrix and brittle crack does not occur, and leaving a cavity on the machined surface. The cutting force reaches its maximum value when particle 2 debonds from the matrix, then particle 2 is embedded in the matrix and forms a chip. For particle 3, the contact part is at the lower-middle part. The local maximum cutting force is bigger than the traction of the particle and the matrix but smaller than the fracture toughness of the particle. Particle 4 is located above the cutting path. The tool only needs to overcome the resistance of cutting matrix and a small part of the matrix–particle traction. Thus, the cutting force value is minimum.

During UEVC, when the tool moves to the same position, the fragmentation degree of particle 1 is greater than that of OC, and the crack extends faster, which penetrates the whole particle at the beginning of contact, as shown in Fig. 12a. Particle 2 is broken, and the fracture line

of the particle is almost along with the tool particle contact position. The rapid splitting of particles causes part of the reinforced particles to remain in the matrix. Thus, no pit remains. With the impact characteristic of UEVC, as shown in Fig. 11, the instantaneous speed is 1250 mm/s when the tool contacts with the workpiece. This value is greater than the OC cutting speed, and machining occurs during only a small part of a cycle, resulting in the tool having more kinetic energy. Therefore, particles 1, 2, and 3 have a greater fracture degree. Particle 1 has smaller fragments than in OC, particles 2 and 3 break heavily, and particle 4 experiences local fracture in the border. The above-mentioned failure forms can be addressed by UEVC, i.e., through multiple processing of a particle that gradually destroys the structure of the particles, which makes the particles easy to break and transform into small fragments, thereby preventing bigger particle fragments from scratching the workpiece matrix. The longitudinal vibration behavior of the tool also has a positive role in the formation of the chips. After the particles are crushed, the broken parts are taken away from the machined surface by the longitudinal movement of the cutter. This behavior reduces the possibility of secondary machining. As shown in Figs. 12b and 12c, the simulation indicates that due to the vertical vibration of the tool in the later stage of the tool rising, the friction force opposite to the initial contact direction takes the chip to move upward and promotes chip outflow so that when the chip thickness formed by the aluminum matrix is about half that of OC, it is taken away from the workpiece.

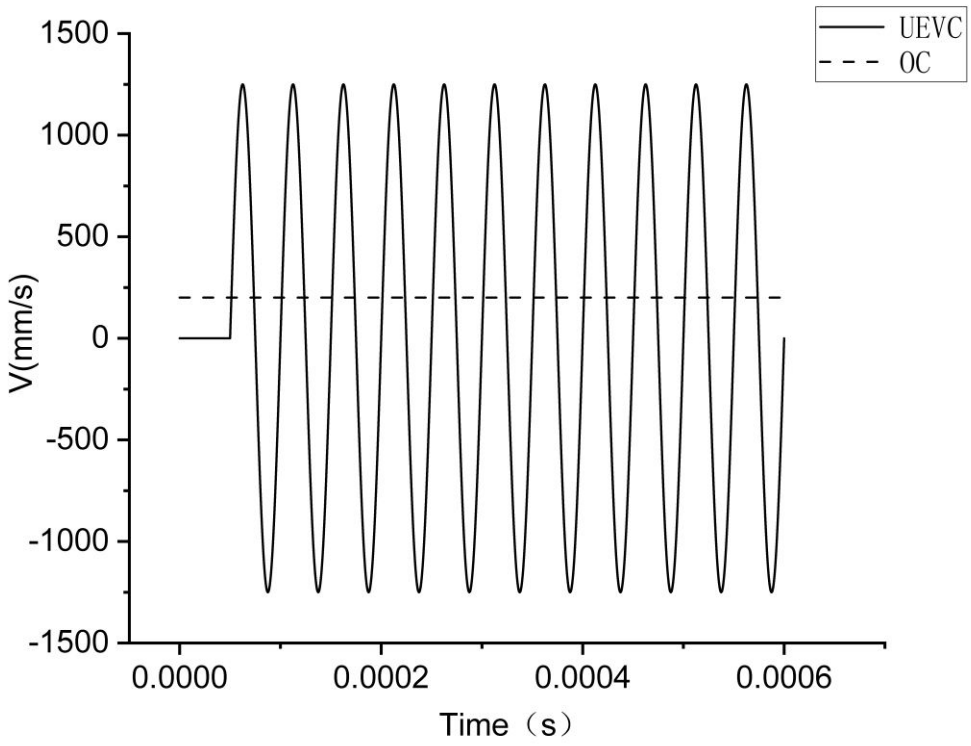

Fig. 11 Variation of tool speed in the cutting speed direction.

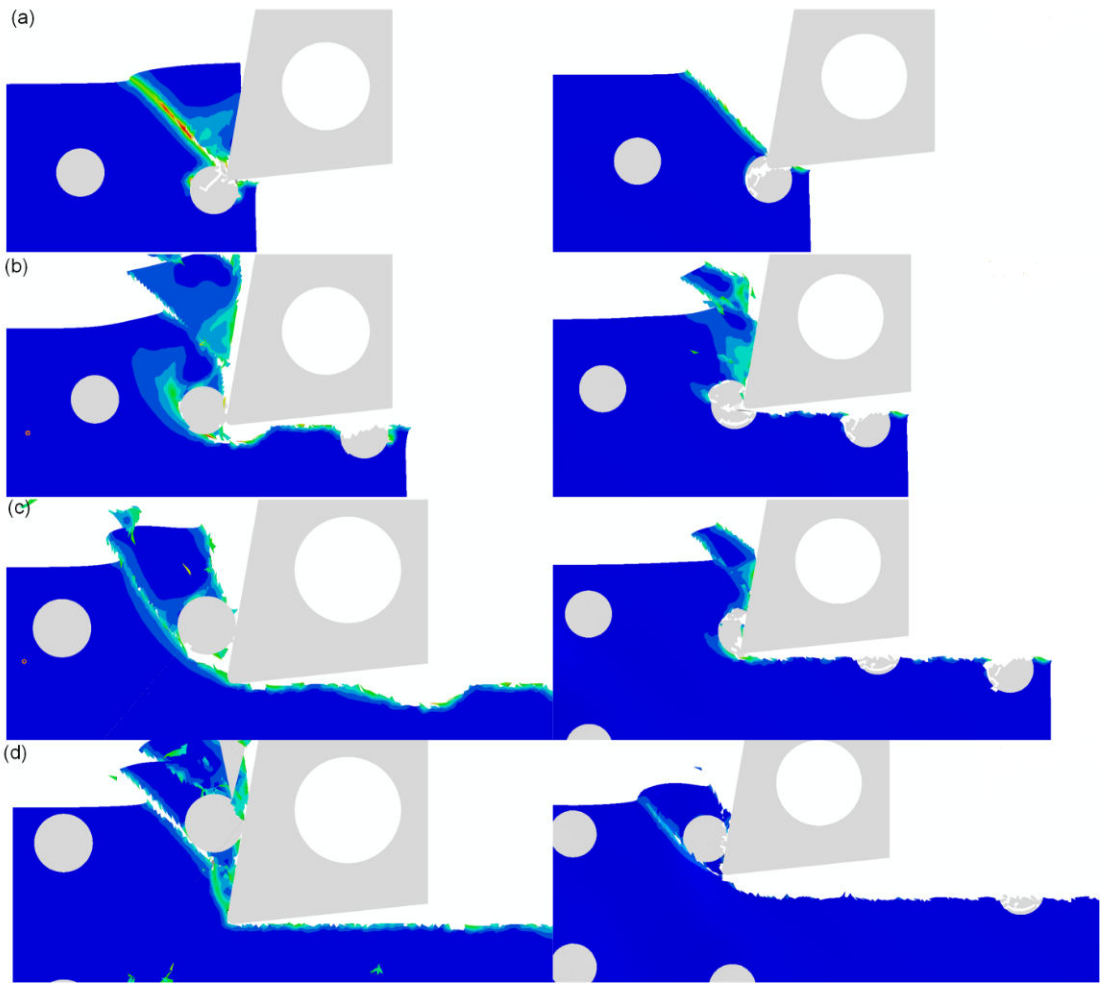

Fig. 12 Simulation at different stages of chip formation in machining of Al/SICp composites. Left is OC and right is UEVC. (a) position at particle 1; (b) position at particle 2; (c) position at particle 3; (d) position at particle 4.

4.3 Distribution of effective stress of ordinary cutting and ultrasonic vibration cutting

Figure 13 shows the von Mises stress distribution contours of the initial stage of tool particle contact. In the two models, the maximum von Mises stress on the workpiece during machining is mainly concentrated in the reinforced particles, which indicates that the supporting reaction force on the tool is mainly from the reinforced particles. The contour figures show the different von Mises stress distribution of the two machining methods. In the process of machining SiCp/Al

with OC, an obvious stress shear band with an irregular shape can be observed when the cutter touches particles 1 and 2. The stress concentration areas in OC are the main shear band, SiC particles in the processing state, the nearby matrix, and other particles. The stress transfer is hindered by the other particles, which means that the particles that are not in contact with the tool also bear greater stress. The load of the former particle transfers to the next particle, which makes the latter debonding occur earlier or causes local fracture, and then affects the subsequent interaction between the tool and the workpiece. However, the von Mises stress distribution of UEVC is concentrated in a very small range. The stress concentration areas are SiC particles and the nearby matrix. No obvious shear band exists, and the high stress concentrate area it does not interfere with other particles when the current particles are processed. The von Mises stress in OC is transferred along the straight line where the tool and SiC particle center of mass are located after the tool contacts with the particle, and the stress transfer range is large. In UEVC, because the instantaneous cutting direction of the tool changes continuously, the von Mises stress transfer direction also changes continuously, which mainly depends on the contact position between the tool movement direction and the particles. Figure 13 shows that the von Mises stress of UEVC at the moment of tool and particle contact is two to seven times that of OC. Thus, particles 1, 2, and 3 achieve fracture toughness, resulting in a large number of cracks and smaller fragments. Figure 14 shows the von Mises stress distribution of the workpiece when the tool retreats. UEVC periodically moves away from the workpiece, thereby decreasing the

effective stress. Different from the continuous contact of chips in OC, most of the time in a cycle, the tool and chip are separated, and no extrusion occurs between them. Therefore, the residual stress of the machined surface of UEVC is less than that of OC, which is reduced to one-quarter to seventh of OC. The difference in the von Mises stress distribution between the two models indicates that the UEVC processing mode changes the stress propagation and distribution mechanism in the cutting process.

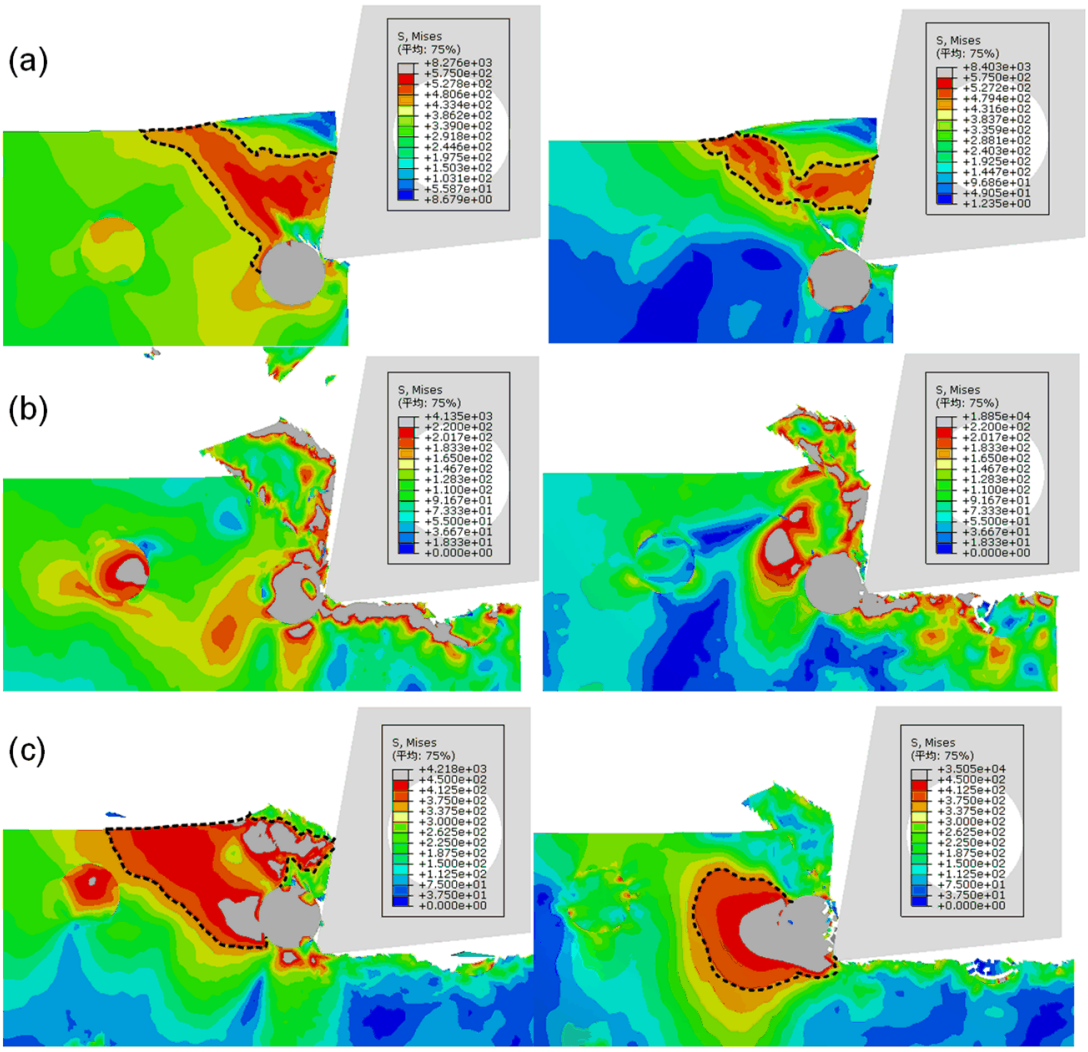

Fig, 13 Simulation of von Mises stress distribution in machining of Al/SiCp composites at (a) stage of machining particle 1; (b) stage of machining particle 2; (c) stage of machining particle 3; Left is OC and right is UEVC.

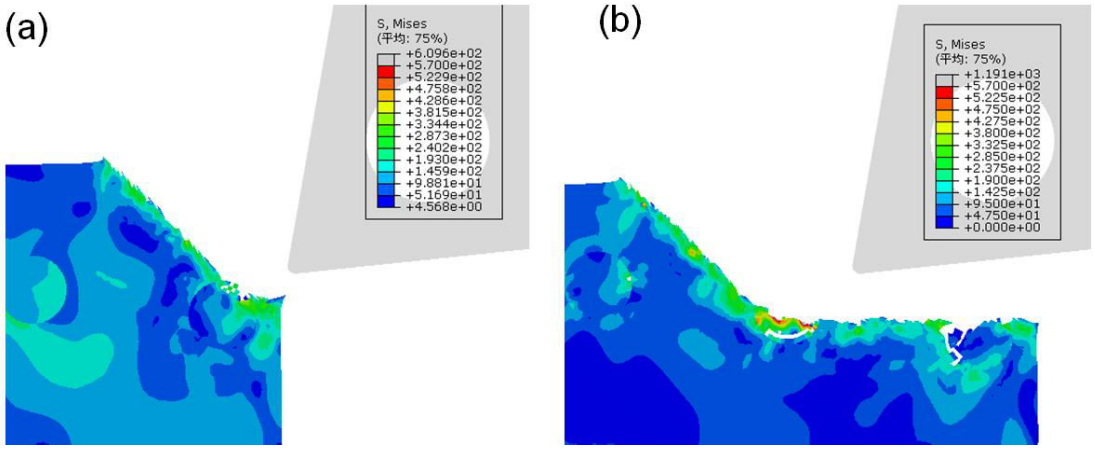

Fig. 14 Simulated von Mises stress distribution at UEVC tool back-off stages; (a) particle 1; (b) particle 2.

4.4 Surface integrity

Different tool–particle interaction behaviors occur during OC and UEVC machining, thereby leading to varying formation mechanisms of the machined surface morphology. Figure 15 shows a colored area that indicates residual stress and shows the structure of the machined surface with or without ultrasonic elliptical vibration under the processing conditions of f = 20 KHz, V = 200 mm/s, A = 10 μm, B = 8 μm, and DOC = 20 μm. The line graph further shows the profile drawn according to the surface height change, and the position and shape of the reinforced particles before fracture are marked with a scatter diagram. The decrease in the machined surface integrity of Al/SiCp can be attributed to excessive strain and secondary damage to the matrix caused by particle fracture and particle debonding. The crack and evolution of SiC particles and the relative position between particles and tool are closely related to the formation of the machined surface, which can be summarized as forming cavity and residual fragment that embedded in the matrix

caused by fracture of particles on the cutting path. Particles function as a cutting tool after debonding and scratching on the machined surface. The particles under the cutting path are pressed into the matrix, thereby increasing the stress or severe plastic deformation on the machined surface.

After particle 1 is broken, the smaller upper part is discharged with the chip, and the larger part remains in the Al matrix. Particle 2 is not destroyed and is completely debonded, but the particles pulled from the Al matrix processed the surface again, which reduced the surface finish and left a pit with a radius of about 0.018 μm, which is 1.8 times of the particle diameter.

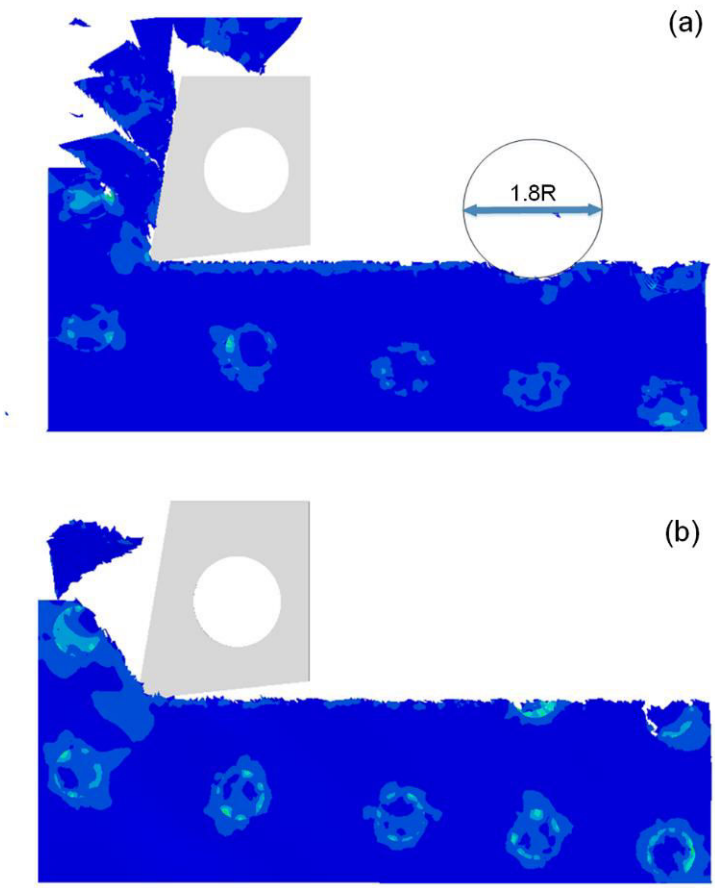

Fig. 15 Simulated surface profile of two methods; (a) OC; (b) UEVC.

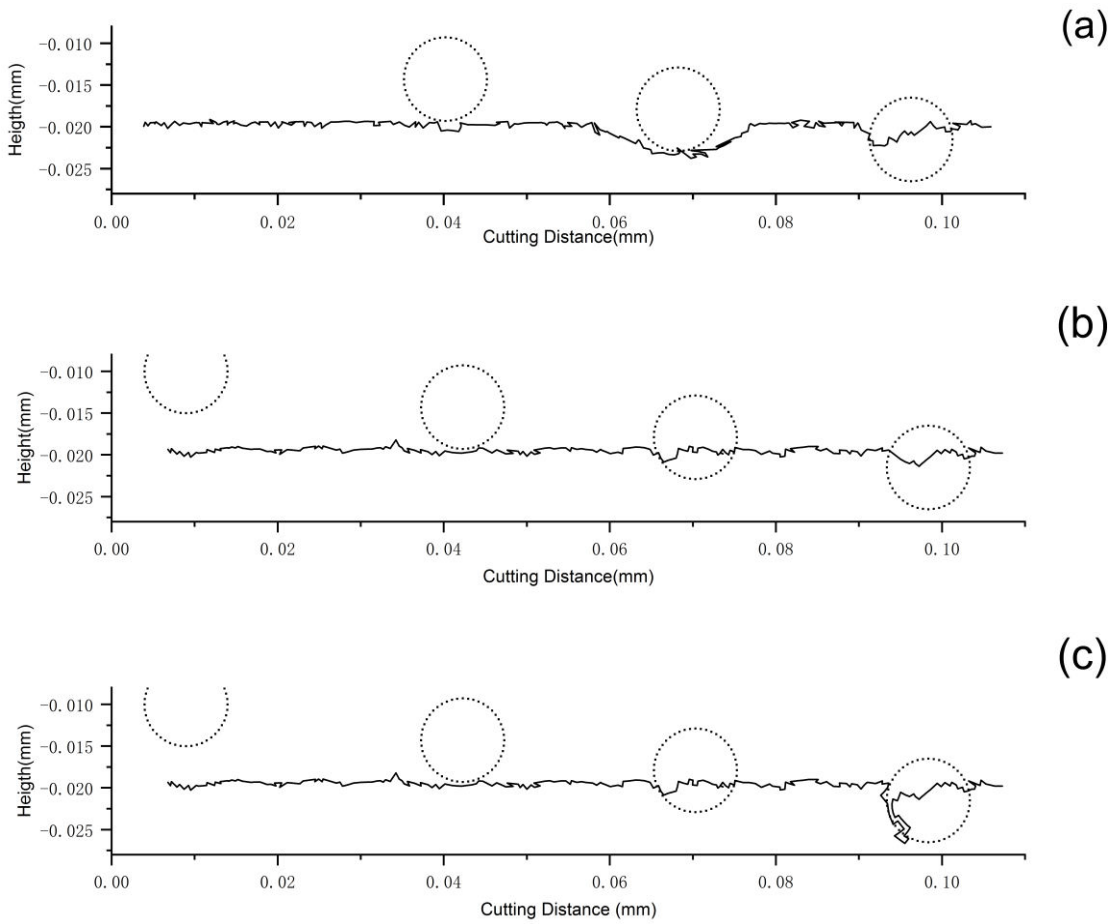

Fig. 16 Extracted from simulated results of the surface profile; (a) OC; (b) UEVC without cavity; (c) UEVC with cavity.

In the UEVC simulation results, the main failure mode of SiC particles is fracture, which does not easily appear secondary processing and scratching. The local fracture of SiC particles will improve the surface finish, but due to the excessive stress, a cavity exists throughout the whole particle, which will have a certain impact on the surface integrity.

In this paper, the arithmetic mean center line of the surface profile is used as the datum line to evaluate the surface roughness parameters, i.e., the area enclosed by the contour of the upper and lower parts, and the datum line is equal. Figure 16

shows the machined surface profiles of OC and UEVC, and the latter is divided into two parts, including cavity or without a cavity. Figure 17 shows the surface roughness Ra of OC and UEVC after machining at the same sampling length. The surface roughness of OC is 875 nm and that of UEVC with cavity is 814 nm, indicating a 7% decrease. If the cavity is not included, then the surface roughness decreases by 60.8%.

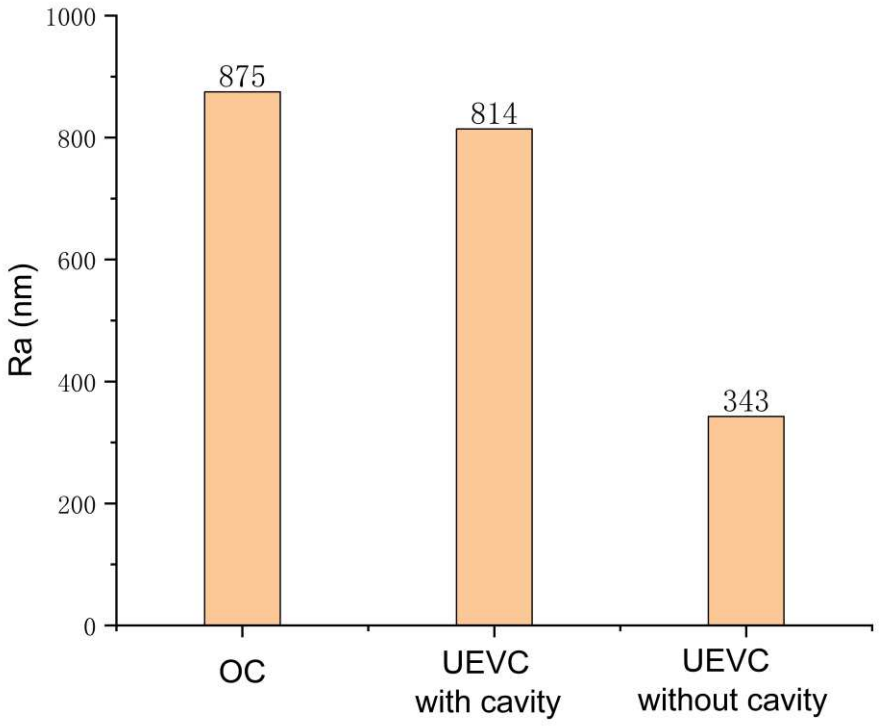

Fig. 17 Comparison of the total surface roughness (Ra) between the OC and UEVC.

Fig. 18 shows the surface roughness value of the matrix, particle 1, and particle 2, which are defined as follows: Particle refers to the intersection of the outer circle contour and the machined surface. The cavity range is shown in the surface contour (Fig. 16(c)). The surface roughness of particle 2 of OC refers to the whole concave

part caused by particle 2, and the matrix refers to the condition without the part described above.

For the matrix, the surface roughness of OC is 615 nm, and that of UEVC is 315nm; the latter is 48% lower than the former. For particle 2, the surface roughness of OC is 1921 nm, and that of UEVC is 372.7 nm; the latter is 80% lower than the former. For particle 1, the surface roughness of OC is 866.4 nm, and that of UEVC is 2526 nm; the latter is 62% higher than the former. Without the cavity, the latter is 20.5% lower than the former.

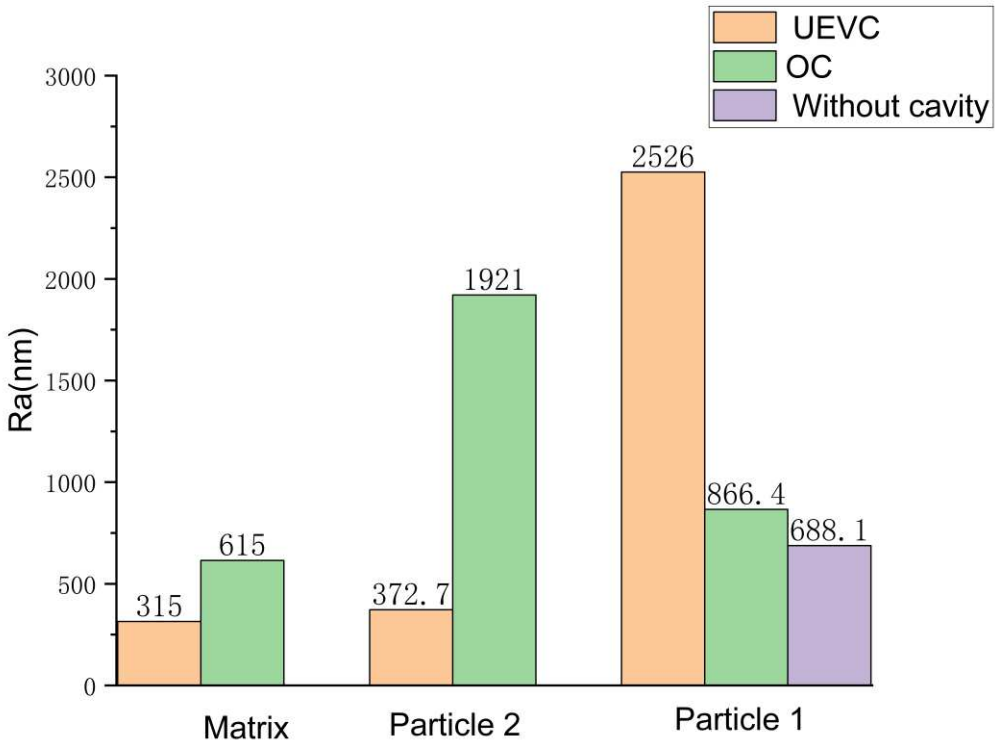

Fig. 18 Comparison of the specific part surface roughness (Ra) between the OC and UEVC.

Generally speaking, the roughness (Ra) of the machined surface of UEVC is better than that of OC when Al/SiCp is processed under the same conditions mainly because OC processing

cannot deal with the secondary processing of unbroken particles on the machined surface. If the cavity is not included, then the advantage is further enhanced.

5. Conclusion

The finite element simulation model of the machining process of Al/SiCpl composites containing cohesive elements is established, and the cutting mechanism of UEVC of Al/SiCp composites is studied. Including the tool particle interaction and its influence on cutting force, chip formation, von Mises stress distribution, and surface roughness. In addition to reducing the average cutting force through periodic contact, the longitudinal motion changes the direction of the thrust force, further reduces the resultant cutting force and promotes chip outflow. The impact effect of UEVC increases the instantaneous cutting speed and kinetic energy of the tool, the von Mises stress distribution is more concentrated and much greater in the UEVC process than in OC, thereby enhancing the break degree of SiC particles, and the residual stress on the machined surface is less than that of OC when the tool is withdrawn, which is conducive to maintaining the integrity of the unfinished part. With the nodal displacement of the two simulation results taken as the surface roughness, UEVC is proven to be better than OC when machining Al matrix and particle 2, however, the high speed impact of tool leads to cavity in SiC particle 1, this phenomenon significantly affects the machined surface quality.

All the conclusions of this article are drawn from the finite element simulation, this paper has its limitations.although todays finite element simulation technology has approached to the actual experiment, there are still differences. The model included cohesive elements can’t simulate the variation of temperature, and there are no research about the cutting parameters’ effect on particle

reinforced metal material composite, so the research content is not perfect. Besides that, the OC model is utilized indirectly to verify the correctness of UEVC model. However, if possible, UEVC experiments under corresponding cutting parameters should be carried out to verify the results.

Declaration

Funding

The authors did not receive support from any organization for the submitted work.

Conflicts of Interest

The authors have no conflicts of interest to declare that are relevant to the content of this article.

Availability of data and material

All data generated or analysed during this study are included in this published article。

Code availability

Not applicable

Ethics approval

The content studied in this article belongs to the field of metal processing, and does not involve humans and animals. This article strictly follows the accepted principles of ethical and professional conduct.

Consent to participate

Not applicable

Consent for publication

Not applicable

Authors' contributions

Wenxiang Chen: investigation; methodology; validation; writing—original draft; Xu Zhang: supervision.

Reference

[1] Davim JP, 2012. Machining of metal matrix composites. London: Springer. p. 1795–803. https://doi.org/10.1007/978-0-85729-938-3.

[2] Pramanik A, Zhang LC, Arsecularatne JA, 2008. Machining of metal matrix composites: effect of ceramic particles on residual stress, surface roughness and chip formation. Int J Mach Tool Manuf. 48:1613-25. https://doi.org/10.1016/j.ijmachtools.2008.07.008.

[3] Tamer Ozben, Erol Kilickap, Orhan Çakir, 2008. Investigation of mechanical and machinability properties of SiC particle reinforced Al-MMC, J Mater Process Technol. 198: 220-225. https://doi.org/10.1016/j.jmatprotec.2007.06.082.

[4] Monaghan J, Brazil D, 1998. Modelling the flow processes of a particle reinforced metal matrix composite during machining. Compos Part A Appl Sci Manuf. 29:87–99. https://doi.org/10.1016/S1359-835X(97)00047-X.

[5] Zhu Y, Kishawy H A, 2005. Influence of alumina particles on the mechanics of machining metal matrix composites[J]. International Journal of Machine Tools and Manufacture. 45(4-5):389-398. https://doi.org/10.1016/j.ijmachtools.2004.09.013.

[6] Chunzheng Duan, Wei Sun, Cheng Fu, Fangyuan Zhang, 2018. Modeling and simulation of tool-chip interface friction in cutting Al/SiCp composites based on a three-phase friction model. Int J Mech Sci. 142-143:384-396. https://doi.org/10.1016/j.ijmecsci.2018.05.014.

[7] Shijin LU, Junjie ZHANG, Zengqiang LI, Jianguo ZHANG, Xiaohui WANG, 2021. Cutting path-dependent machinability of SiCp/Al composite under multi-step ultra-precision diamond cutting, Chinese J Aeronaut. 34: 241-252. https://doi.org/10.1016/j.cja.2020.07.039.

[8] Wu Q, Si Y, Wang G-S, Wang L, 2016. Machinability of a silicon carbide particle-reinforced

metal matrix composite. RSC Adv. 6:21765 – 21775. https://doi.org/10.1039/C6RA00340K.

[9] Wang T, Xie L, Wang X, 2015. Simulation study on defect formation mechanism of the machined surface in milling of high volume fraction SiCp/Al composite. Int J Adv Manuf Technol. 79:1185 – 1194. https://doi.org/10.1007/s00170-015-6876-x.

[10] Wang, Y., Liao, W., Yang, K. et al. Investigation on cutting mechanism of SiCp/Al composites in precision turning. Int J Adv Manuf Technol 100, 963 – 972 (2019). https://doi.org/10.1007/s00170-018-2650-1.

[11] Shamoto Eiji, Moriwaki Toshimichi, 1994. Study on Elliptical Vibration Cutting. CIRP Ann-Manuf Techn. 43:35-38. https://doi.org/10.1016/S0007-8506(07)62158-1.

[12] Zhang, J., Wang, D, 2019. Investigations of tangential ultrasonic vibration turning of Ti6Al4V using finite element method. Int J Mater Form. 12:527-267. https://doi.org/10.1007/s12289-018-1402-y.

[13] Gao J , Jin X, 2019. Effects of Ultrasonic Vibration Assistance on Chip Formation Mechanism in Cutting of Ti-6Al-4V. Journal of Manufacturing Science and Engineering. 141(12):1-21. https://doi.org/10.1115/1.4045129.

[14] He, Y., Zou, P., Zhu, WL. et al, 2017. Ultrasonic elliptical vibration cutting of hard materials: simulation and experimental study. Int J Adv Manuf Technol. 91:363-374. https://doi.org/10.1007/s00170-016-9716-8.

[15] A.V. Mitrofanov, V.I. Babitsky, V.V, 2004. Silberschmidt. Finite element analysis of ultrasonically assisted turning of Inconel 718. J Mater Process Tech. 153:233-239. https://doi.org/10.1016/j.jmatprotec.2004.04.299.

[16] Wei Bai, Ronglei Sun, Jürgen Leopold, Vadim V, 2017. Silberschmidt. Microstructural evolution of Ti6Al4V in ultrasonically assisted cutting: Numerical modelling and experimental analysis. Ultrasonics. 78:70-82. https://doi.org/10.1016/j.ultras.2017.03.005.

[17] Zheng W, Wang Y, Zhou M, et al, 2018. Material deformation and removal mechanism of SiCp/Al composites in ultrasonic vibration assisted scratch test. Ceramics International. 15133-15144. https://doi.org/10.1016/j.ceramint.2018.05.150.

[18] Tong, J., Zhao, J., Chen, P. et al, 2020. Effect of ultrasonic elliptical vibration turning on the microscopic morphology of aluminum alloy surface. Int J Adv Manuf Technol. 106:1397-1407. https://doi.org/10.1007/s00170-019-04463-x.

[19] Tan R, Zhao X, Sun T, Zou X, Hu Z. Experimental Investigation on Micro-Groove Manufacturing of Ti-6Al-4V Alloy by UsingUltrasonic Elliptical Vibration Assisted Cutting. Materials (Basel) 2019;12(19). https://doi.org/10.3390/ma12193086.

[20] Junjie Zhang, La Han, Jianguo Zhang, Haiying Liu, Yongda Yan, Tao Sun, 2019. Brittle-to-ductile transition in elliptical vibration-assisted diamond cutting of reaction-bonded

silicon carbide. J Manuf Process 45:670-681. https://doi.org/10.1016/j.jmapro.2019.08.005.

[21] Daxi Geng, Yihang Liu, Zhenyu Shao, Mingliang Zhang, Xinggang Jiang, Deyuan Zhang, 2020. Delamination formation and suppression during rotary ultrasonic elliptical machining of CFRP, Composites Part B: Engineering. 183 107698, https://doi.org/10.1016/j.compositesb.2019.107698.

[22] Gi Dae Kim, Byoung Gook Loh, 2008. Journal of Micromechanics and Microengineering Characteristics of elliptical vibration cutting in micro-V grooving with variations in the elliptical cutting locus and excitation frequency. J Micromech Microeng. 18 025002. https://doi.org/10.1088/0960-1317/18/2/025002.

[23] Xiangyu Teng, Wanqun Chen, Dehong Huo, Islam Shyha, Chao Lin, 2018. Comparison of cutting mechanism when machining micro and nanoparticles reinforced SiC/Al metal matrix composites.Compos Struct. 203:636-647. https://doi.org/10.1016/j.compstruct.2018.07.076.

[24] Chinmaya R. Dandekar, Yung C. Shin, 2013. Multi-scale modeling to predict sub-surface damage applied to laser-assisted machining of a particulate reinforced metal matrix composite, Int J Mater Process Technol. 213:153-160. https://doi.org/10.1016/j.jmatprotec.2012.09.010.

[25] Umer, U., Ashfaq, M., Qudeiri, J.A. et al, 2015. Modeling machining of particle-reinforced aluminum-based metal matrix composites using cohesive zone elements. Int J Adv Manuf Technol. 78:1171-1179. https://doi.org/10.1007/s00170-014-6715-5.